Microstructure of Block Copolymers near Selective Surfaces: Theoretical Predictions and Configurational-Bias Monte Carlo Simulation

Dapeng Cao and Jianzhong Wu*

Department of Chemical and Environmental Engineering, University of California, Riverside, California 92521

Received August 3, 2004; Revised Manuscript Received November 15, 2004

ABSTRACT: We report a new density functional theory (DFT) for block copolymers and its performance for representing the microscopic structure has been tested with the configurational-bias Monte Carlo simulation. The segmental density profiles are calculated for systems containing short block copolymers, represented by tangent-sphere square-well chains of sequences "AABB", "AAAABBBB", "ABBBBA", "ABBBBBBA", "BBAABB", and "BBBBAABBBB" confined in slit pores where the planar surfaces attract "A" segments but repel "B" segments. The detailed segmental density profiles are calculated for block copolymers confined in slit pores where the planar surfaces attract "A" segments but repel "B" segments. For all conditions considered, the microscopic structures predicted by the DFT are in excellent agreement with the simulation results. Interesting loop and tail conformations of the block copolymers are observed near the selective surfaces. The effects of surface energy, chain length, and copolymer backbone structures on the microscopic segregation of "AB" segments are also investigated.

1. Introduction

Block copolymers consist of at least two parts typically with stark different physiochemical properties. When they are exposed to a surface that preferentially attracts one part but repels the other, a rich variety of microscopic structures may arise, depending on the chain architecture and the energetic/chemical nature of the surface.[1,2] These structures are directly related to the performance of copolymers in a number of important technological applications, including stabilization of nanoparticle dispersions[3,4] and copolymer-based lithography and photonic materials.[5]

Early theoretical work for understanding the interfacial properties of block copolymers is primarily based on the phenomenological Landau expansions[6] or the self-consistent-field theory (SCFT),[7] following the great success of similar approaches for describing various microphase separations in block copolymer melts.[8] Fredrickson published the first notable work in this area by extending Leibler's formulation of the free energy for weak segregated block copolymer melts to similar systems in contact with a free surface or a solid substrate.[9] The oscillatory density profiles and surface-induced ordering predicted by the mean-field theory are in good agreement with experiments.[10] On the other hand, Fleer and co-workers formulated a lattice-based SCFT for the adsorptions of block copolymers and examined the detailed segmental density profiles, loop and tail structures, and adsorption isotherms of both di- and triblock copolymers.[11,12] Enormous work has been published since early 1990s on the interfacial activity of block copolymers between immiscible homopolymers, motivated by the creation of useful polymer blends with unique combination of the desired properties of individual components. In particular, the lattice-based SCFT was extensively used to examine surface tension, micellization, interfacial density profiles, and bulk phase transitions in block copolymer/homopolymer blends.[13,14] Quantitative agreement between theory and neutron reflectivity experiments was achieved for the composition profiles and interfacial widths of block copolymer domains between immiscible homopolymers.[15] Another area that attracts considerable theoretical interest is on the phase transitions or morphologic changes in block copolymer thin films at either uniform or patterned surfaces. Various versions of SCFT and Ginzburg−Landau-type approaches have been applied to constructing the thickness-dependent phase diagrams of diblock and, more recently, triblock copolymer films.[16−26] Good agreement between theory and Monte Carlo simulation was found.[27]

SCFT and Landau expansions share a common limitation when a connection between the model parameters and the chemical details of copolymers is of direct concern. Indeed, these oversimplified theories are often insufficient to capture the segment-level behavior of block copolymer systems under different thermodynamic conditions. As encountered in the application of the Flory−Huggins theory for representing the phase diagrams of bulk polymeric systems, the parameters appeared in SCFT or Ginzburg−Landau theories only have a loose connection with the intermolecular forces, and they often vary with the system conditions including temperature and pressure. In principle, such limitation can be avoided by applying atomistic molecular dynamics or Monte Carlo simulations by taking into account the details of chemical structure as well as interaction potentials. However, because of the large time and length scales pertinent to copolymer systems, fully atomistic molecular simulations remain out of reach for most realistic cases. An alternative approach, following the mathematic framework of classical density functional theory (DFT), may fill the gap. First introduced by Chandler, McCoy, and Singer (CMS),[28] for polymeric systems DFT has been applied to bulk and inhomogeneous polymeric systems for studying phase transitions, interfacial properties, and inter- and intramolecular correlations.[29−41] Two common approaches

* Corresponding author. E-mail: jwu@engr.ucr.edu.

10.1021/ma048394s CCC: $30.25
Published on Web 01/11/2005

have been used to derive the free energy functional: One follows CMS's original framework based on the quadratic density expansion of the free energy with respect to a reference of ideal system. This approach requires as the input the direct correlation functions from the polymer integral-equation theory (i.e., PRISM[42]) and the intramolecular correlation functions from a single-chain Monte Carlo simulation.[28] The second approach is based on the exact formalism for the ideal part of the free energy functional and a generalized first-order perturbation theory. Whereas the ideal part retains the details of bond connectivity, the contributions due to all nonbonded inter- and intramolecular interactions are taken into account using a weighted density approximation for the short-ranged forces and the first-order perturbation theory for chain correlations. The second approach was initially introduced by Kierlik and Rosinburg[29] based on an earlier work by Woodward.[30] An improved version was recently developed for free-joined chains[34] and for semiflexible polymers.[43] In comparison with SCFT or other coarse-grained approaches, DFT preserves more information on the length scale of a monomer or statistical repeating unit. The same theoretical framework can be applied to both bulk and interfacial properties with a single set of molecular parameters. Furthermore, DFT can be systematically extended to complicated polymeric systems that involve a variety of intermolecular interactions, such as hydrogen bonding and electrostatics.

Early formulism of DFT for copolymer systems, including the one by Melenkevitz and Muthukumar[31] and that by McMullen and Freed,[32] was heavily influenced by SCFT and Landau expansions for the selection of the reference system or for the formulation of the free energy functional. Such connection remains apparent in numerous recent publications of so-called dynamic density functional theory or Mesodyn.[44,45] Most recent DFT theories, however, directly adopt the segmental-level intermolecular forces following either the CMS approach[46−49] or the generalized thermodynamic perturbation theory.[29,30,34] The former approach has been used to describe the phase transitions in symmetric block copolymer melts,[47] thin films,[48,49] and vapor−liquid nucleation of short amphiphilic chains.[50] Recently, Frink and co-workers demonstrated that CMS-DFT is able to capture the detailed morphology and microscopic phase transitions of diblock copolymer thin films as a function of film thickness, in good agreement with previous SCF calculations and experiments.[49]

In this work, a new DFT for block copolymers is proposed, and its performance for representing the microscopic structures is tested with the configurational-bias Monte Carlo simulation for relatively short copolymer chains. Following our previous work for homopolymers and inhomogeneous simple fluids, we formulate the free energy functional in terms of a modified fundamental measure theory for the excluded volume effects,[51] a generalized first-order thermodynamic perturbation theory for chain correlations,[34] and a mean-field approximation for the van der Waals attractions. Along with Monte Carlo simulations, this new theory is used to examine the microstructures and conformation of six short block copolymers confined in slit pores with discriminating walls for different segments. For numerical comparison between theory and simulations, we focus on short chains because of the computational limitation of simulations rather than DFT.

The remainder of this paper is organized as the following. Section 2 presents the molecular models and force fields used in this work. The details of the density functional theory for block copolymers are given in section 3. Section 4 briefly outlines the configurational-bias Monte Carlo simulation method. In section 5, we examine the results from DFT and simulations for the microstructures of block copolymers confined in slit pores with selective walls. Finally, some conclusive remarks are drawn in section 6.

2. Molecular Models

All block copolymers considered in this work are represented by tangent-sphere chains consisting of two types of segments, designated by "A" and "B". These segments have the same size but different van der Waals attractions described by a square-well (SW) potential:

$$\varphi_{ij}(r) = \begin{cases} \infty & r < \sigma \\ -\epsilon_{ij} & \sigma \le r \le \gamma\sigma \\ 0 & r > \gamma\sigma \end{cases} \tag{1}$$

where σ is the segment diameter, $\gamma\sigma$ is the square-well width, and ϵ_{ij} is an energy parameter with the indexes i and j standing for segments "A" or "B". Throughout this work, the attractive width is fixed at $\gamma = 1.2$. As in a standard off-lattice model for polymers, this minimum model retains only the basic features of a copolymer: the excluded-volume effect, chain connectivity, and specific interactions between different segments. However, as discussed later, the formulation of DFT is not limited to this oversimplified model.

For direct comparison between theory and simulations, we consider the microscopic structures of various short block copolymers or amphiphilic molecules confined in a slit pore where the slit walls attract "A" segments but repel "B" segments. Specifically, three types of block copolymers are investigated: (1) symmetric diblock copolymers with the sequence of "AABB" or "AAAABBBB", (2) copolymers with the end sites preferred to the surfaces ("ABBBBA", "ABBBBBBA"), and (3) triblock copolymers with the middle sites preferred to the surfaces ("BBAABB", "BBBBAABBBB"). Copolymers of short chain length are considered in this work because of the numerical efficiency for Monte Carlo simulations.

The interaction between a segment and a slit wall is also represented by a square-well potential

$$\varphi_{iW}^{\text{att}}(z) = \begin{cases} -\epsilon_{iW} & 0 < z < w \\ 0 & \text{otherwise} \end{cases} \tag{2}$$

where z is the perpendicular distance from the surface, i = A or B, w is the width of the surface potential, and ϵ_{iW} stands for the wall energy. In this work, the surface width parameter is fixed at $w = \sigma$. All surface interactions are terminated at $w = \sigma$, which is referred to as the range of surface energy. Because the wall prefers segment "A" and abhors segment "B", the surface creates an attractive well for "A" segments and a repulsive shoulder for "B" segments. Therefore, ϵ_{AW} is always positive and ϵ_{BW} is always negative.

3. Density Functional Theory

3.1. Helmholtz Energy Functional. The Helmholtz energy functional of a polymeric system can be ex-

pressed in terms of that corresponding to a system of ideal chains where all nonbonded interactions are turned off and an excess part due to both inter- and intramolecular nonbonded interactions

$$F[\rho_M(\mathbf{R})] = F_{id}[\rho_M(\mathbf{R})] + F_{ex}[\rho_M(\mathbf{R})] \quad (3)$$

where $\mathbf{R}$ is a composite vector ($\mathbf{r}_1$, $\mathbf{r}_2$, ..., $\mathbf{r}_M$) representing the positions of individual segments, and $\rho_M(\mathbf{R})$ stands for a multidimensional density profile.

The Helmholtz energy functional of ideal chains with a bonding potential specified by $V_{bond}(\mathbf{R})$ is known exactly

$$\beta F_{id}[\rho_M(\mathbf{R})] = \int d\mathbf{R}\, \rho_M(\mathbf{R})[\ln \rho_M(\mathbf{R}) - 1] + \beta \int d\mathbf{R}\, \rho_M(\mathbf{R})\, V_{bond}(\mathbf{R}) \quad (4)$$

For tangent-sphere chains considered in this work, the bonding potential $V_{bond}(\mathbf{R})$ is related to the Dirac delta function by

$$\exp[-\beta V_{bond}(\mathbf{R})] = \prod_{i=1}^{M-1} \frac{\delta(|\mathbf{r}_{i+1} - \mathbf{r}_i| - \sigma)}{4\pi\sigma^2} \quad (5)$$

where M denotes the number of segments for each molecule and $\mathbf{r}$ represents a segmental position. In eqs 4 and 5, $\beta = (kT)^{-1}$ with k standing for the Boltzmann constant and T for temperature. Because eq 4 is true for an arbitrary bonding potential, the DFT described here is able to take into account the chemical details of a polymeric system, at least in principle.

The key assumption in our density functional theory is that the excess Helmholtz energy functional is exclusively determined by the density profiles of individual segments and the structure of bond connectivity. In other words, for a given configuration of molecules represent by the composite vector $\mathbf{R}$, the excess Helmholtz energy is not directly related to the details of bonding potentials. Therefore, in terms of the excess Helmholtz energy functional, the reference system is a monomeric fluid with the same density distributions. For the block copolymers considered in this work, the nonbonded intersegmental interactions consist of two parts: hard-sphere repulsions and van der Waals attractions. Correspondingly, the excess Helmholtz energy functional can be formally written as[43]

$$F_{ex}[\rho_A(\mathbf{r}),\rho_B(\mathbf{r})] = F_{hs} + F_{att} + F_{chain} \quad (6)$$

where $\rho_A(\mathbf{r})$ and $\rho_B(\mathbf{r})$ are the density profiles of segments A and B. The first two terms on the right-hand side of eq 6 represent the excess Helmholtz energies due to the hard-sphere repulsions and van der Waals attractions, respectively. These two terms depend only on the segmental densities. Conversely, F_{chain} takes into account the effect of chain connectivity on the correlation between segments that, in the framework of the first-order perturbation theory, can be related to the segmental densities and the backbone structure (but not the bonding potentials).

Following our previous work for homopolymers,[34,35] the hard-sphere part of the Helmholtz energy functional is represented by a modified fundamental measure theory[52]

$$\beta F_{hs} = \int d\mathbf{r} \left\{ -n_0 \ln(1 - n_3) + \frac{n_1 n_2 - \mathbf{n}_{V_1}\cdot\mathbf{n}_{V_2}}{1 - n_3} + (n_2^3/3 - n_2 \mathbf{n}_{V_2}\cdot\mathbf{n}_{V_2}) \left[\frac{\ln(1 - n_3)}{12\pi n_3^2} + \frac{1}{12\pi n_3 (1 - n_3)^2} \right] \right\} \quad (7)$$

where $n_\alpha(\mathbf{r})$, $\alpha = 0, 1, 2, V_1, V_2$ are weighted densities defined by Rosenfeld.[53] These scalar and vector weighted densities are given by

$$n_\alpha(\mathbf{r}) = \sum_j n_{\alpha j}(\mathbf{r}) = \sum_j \int \rho_j(\mathbf{r}')\, \omega_j^\alpha(\mathbf{r} - \mathbf{r}')\, d\mathbf{r}' \quad (8)$$

where $\bar{\omega}_j^\alpha$ ($\alpha = 0, 1, 2, 3, V_1, V_2$) are six weight functions, and the subscript $j = 1, 2$ denotes the index of segments "A" and "B". Among the six weight functions, three are directly related to the geometry of a spherical particle:[53]

$$\omega_j^2(r) = \delta(\sigma/2 - r); \quad \omega_j^3(r) = \Theta(\sigma/2 - r); \quad \omega_j^{V_2}(\mathbf{r}) = (\mathbf{r}/r)\delta(\sigma/2 - r) \quad (9)$$

where $\Theta(r)$ is the Heaviside step function, $\delta(r)$ is the Dirac delta function, $\omega_j^2(r)$ and $\omega_j^3(r)$ represent the particle surface area and volume, respectively, and $\omega_j^{V_2}(\mathbf{r})$ denotes the gradient across a sphere in the $\mathbf{r}$ direction. The other weight functions are proportional to the three geometric functions

$$\omega_j^0(r) = \omega_j^2(r)/(\pi\sigma^2); \quad \omega_j^1(r) = \omega_j^2(r)/(2\pi\sigma); \quad \omega_j^{V_1}(\mathbf{r}) = \omega_j^{V_2}(\mathbf{r})/(2\pi\sigma) \quad (10)$$

All weight functions are independent of the density profiles.

The excess Helmholtz energy functional due to the chain connectivity is given by a generalized first-order perturbation theory[34]

$$\beta F_{chain} = \int d\mathbf{r}\, \frac{1 - M}{M} n_0 \xi \ln y^{hs}(\sigma, n_\alpha) \quad (11)$$

where $\xi = 1 - \mathbf{n}_{V_2}\cdot\mathbf{n}_{V_2}/n_2^2$ is defined as an inhomogeneous factor and $y^{hs}(\sigma,n_\alpha)$ is the contact value of the cavity correlation function between segments

$$y^{hs}(\sigma, n_\alpha) = \frac{1}{1 - n_3} + \frac{n_2 \xi \sigma}{4(1 - n_3)^2} + \frac{n_2^2 \xi \sigma}{72(1 - n_3)^3} \quad (12)$$

Equation 11 is not directly related to the bonding potentials of polymeric molecules that have been already included in eq 4. This term takes into account the effect of chain connectivity on the nonbonded interactions between polymeric segments. If the density profiles are everywhere uniform, eqs 11 and 12 reduce to the first-order thermodynamic perturbation theory of bulk fluids.[54,55]

Finally, the excess Helmholtz energy functional due to van der Waals attractions, βF_{ex}^{att}, is represented by a mean-field approximation

$$\beta F_{ex}^{att} = \frac{1}{2} \int\int d\mathbf{r}\, d\mathbf{r}' \sum_{i,j=A,B} \rho_i(\mathbf{r})\, \rho_j(\mathbf{r})\, \beta \varphi_{ij}^{att}(|\mathbf{r} - \mathbf{r}'|) \quad (13)$$

where $\varphi_{ij}^{att}(r)$ is described in eq 1. We have shown in a

recent work that the mean-field approximation is quantitatively accurate for polymers near attractive walls.[43]

As in most DFT approaches, essentially the same formulism is applicable to both homopolymers and copolymers. Despite the relative simplicity of the Helmholtz energy functionals given by eqs 7, 11, and 13, we have shown in our previous work that the DFT is remarkably accurate for predicting the microscopic structures and thermodynamic properties of homopolymers.[34,35] Furthermore, similar equations are applicable to copolymers consisting of segments of different size or mixtures of polymers and block copolymers.

3.2. Euler−Lagrange Equation. At equilibrium, the molecular density profile $\rho_M(\mathbf{R})$ can be solved by minimization of the grand potential

$$\Omega[\rho_M(\mathbf{R})] = F[\rho_M(\mathbf{R})] + \int [\psi_M(\mathbf{R}) - \mu_M]\rho_M(\mathbf{R})\, \mathrm{d}\mathbf{R} \tag{14}$$

where μ_M is the chemical potential of the copolymer chain, which can be calculated from the corresponding equation of state for bulk fluids

$$\beta\mu_M = \ln \rho_M + M\beta\mu_M^{\mathrm{hs,bulk}}(\rho_{\mathrm{bulk}}) + (1 - M)\left[\ln y^{\mathrm{hs,bulk}}(\sigma) + \rho_{\mathrm{bulk}} \frac{\partial \ln y^{\mathrm{hs,bulk}}(\sigma)}{\partial \rho_{\mathrm{bulk}}}\right] + \sum_{\substack{i\in \mathrm{AorB} \\ j\in \mathrm{AorB}}} (-4\pi/3)(\lambda^3 - 1)\epsilon^*_{ij}\rho_{\mathrm{bulk}} x_i x_j \sigma^3 \tag{15}$$

where $\rho_{\mathrm{bulk}} = M\rho_M$ is the total bulk densities of segments "A" and "B", and $\mu^{\mathrm{hs,bulk}}$ is the excess chemical potential of hard sphere represented by Carnahan−Starling equation of state. x_A (or x_j) is the molar fraction of segment "i (or j)" where i (or j) denotes the index of segments "A" or "B". In eq 14, $\psi_M(\mathbf{R})$ is the external potential exerting on individual segments.

Following the variational principles, the stationary condition of the grand potential satisfies

$$\frac{\delta\Omega[\rho_M(\mathbf{R})]}{\delta\rho_M(\mathbf{R})} = 0 \tag{16}$$

Once we have the molecular density profile $\rho_M(\mathbf{R})$, the segmental densities are calculated from

$$\rho_{\mathrm{AorB}}(\mathbf{r}) = \sum_{j\in \mathrm{AorB}} \rho_{sj}(\mathbf{r}) = \sum_{j\in \mathrm{AorB}} \int \mathrm{d}\mathbf{R}\, \delta(\mathbf{r} - \mathbf{r}_j)\, \rho_M(\mathbf{R}) \tag{17}$$

Substitution of eqs 3 and 14 into eq 16 yields the Euler−Lagrange equation

$$\rho_M(\mathbf{R}) = \exp[\beta\mu_M - \beta V_{\mathrm{bond}}(\mathbf{R}) - \beta\sum_{j\in \mathrm{A}} \lambda_{\mathrm{A}}(\mathbf{r}_j) - \beta\sum_{k\in \mathrm{B}} \lambda_{\mathrm{B}}(\mathbf{r}_k)] \tag{18}$$

where $\rho_j(\mathbf{r})$ stands for the local density of segment j denoting the index of segment "A" and "B"; the self-consistent field λ is related to the excess Helmholtz energy functional F_{ex} and the external potential for individual segments φ_A and φ_B:

$$\lambda_{\mathrm{A}}(\mathbf{r}_j) = \frac{\delta F_{\mathrm{ex}}}{\delta\rho_{\mathrm{A}}(\mathbf{r}_j)} + \varphi_{\mathrm{A}}(\mathbf{r}_j) \tag{19a}$$

$$\lambda_{\mathrm{B}}(\mathbf{r}_k) = \frac{\delta F_{\mathrm{ex}}}{\delta\rho_{\mathrm{B}}(\mathbf{r}_k)} + \varphi_{\mathrm{B}}(\mathbf{r}_k) \tag{19b}$$

Combining eq 17 and eq 18, we have a set of coupled integral equations for the segmental density profiles

$$\rho_{si}(\mathbf{r}) = \int \mathrm{d}\mathbf{R}\, \delta(\mathbf{r} - \mathbf{r}_i) \exp[\beta\mu_M - \beta V_{\mathrm{bond}}(\mathbf{R}) - \beta\sum_{j\in \mathrm{A}} \lambda_{\mathrm{A}}(\mathbf{r}_j) - \beta\sum_{k\in \mathrm{B}} \lambda_{\mathrm{B}}(\mathbf{r}_k)] \tag{20}$$

For block copolymers confined in a slit pore, the density distribution varies only in the direction perpendicular to the surface (z), i.e., $\rho_{si}(\mathbf{r}) = \rho_i(z)$. In this case, the average segmental densities are given by

$$\rho_{\mathrm{A}}(z) = \exp(\beta\mu_M)\sum_{i=\mathrm{A}} G^i_{\mathrm{L}}(z) \exp[-\beta\lambda_i(z)] G^i_{\mathrm{R}}(z) \tag{21}$$

$$\rho_{\mathrm{B}}(z) = \exp(\beta\mu_M)\sum_{i=\mathrm{B}} G^i_{\mathrm{L}}(z) \exp[-\beta\lambda_i(z)] G^i_{\mathrm{R}}(z) \tag{22}$$

where $G^i_{\mathrm{L}}(z)$ and $G^i_{\mathrm{R}}(z)$ respectively are the left and right recurrence functions

$$G^i_{\mathrm{L}}(z) = \frac{1}{2\sigma}\int_{z-\sigma}^{z+\sigma} \exp[-\beta\lambda_{i-1}(z)] G^{i-1}_{\mathrm{L}}(z)\, \mathrm{d}z \tag{23}$$

$$G^i_{\mathrm{R}}(z) = \frac{1}{2\sigma}\int_{z-\sigma}^{z+\sigma} \exp[-\beta\lambda_{i+1}(z)] G^{i+1}_{\mathrm{R}}(z)\, \mathrm{d}z \tag{24}$$

with $G^1_{\mathrm{L}}(z) = 1$ and $G^M_{\mathrm{R}}(z) = 1$, and $i = 1, 2, \ldots, M$. Equations 21 and 22 can be solved by standard Picard iteration.[34] Unlike that for homopolymers, the left and right recurrence functions for copolymers bear no symmetry because the Boltzmann factors $\exp[-\beta\lambda_i(z)]$ depend on the identity of the segment "A" or "B".

4. Configurational-Bias Monte Carlo Simulation

To test the performance of our DFT, we carry out configurational-bias canonical Monte Carlo simulations for relatively short copolymers confined in slit pores.[56] For a given pore width and a polymer packing fraction η, the simulation box contains at least 50 copolymer chains. The period boundary conditions are applied to the x and y directions of the simulation box; the box length in the z direction is fixed by the pore width. The recoil−growth algorithm is used to generate the initial polymer configurations, followed by translational, rotational, and configurational-biased (including crankshaft, chain regrowing, and cut rebridging) Monte Carlo moves.[56,57] The different methods for Monte Carlo updates are allocated approximately with the same frequency. Each simulation runs 1×10^7 Monte Carlo cycles, with the first half for the system to reach equilibrium whereas the second half for evaluating the ensemble averages.

5. Results and Discussion

To facilitate a direct comparison between the DFT and configurational-bias Monte Carlo (CBMC) simulations, we consider short diblock and triblock copolymers consisting of "A" and "B" segments confined in slit pores. The confining surfaces attract the "A" segments but repel the "B" segments. In all Monte Carlo simulations, the average packing fraction of copolymers inside the

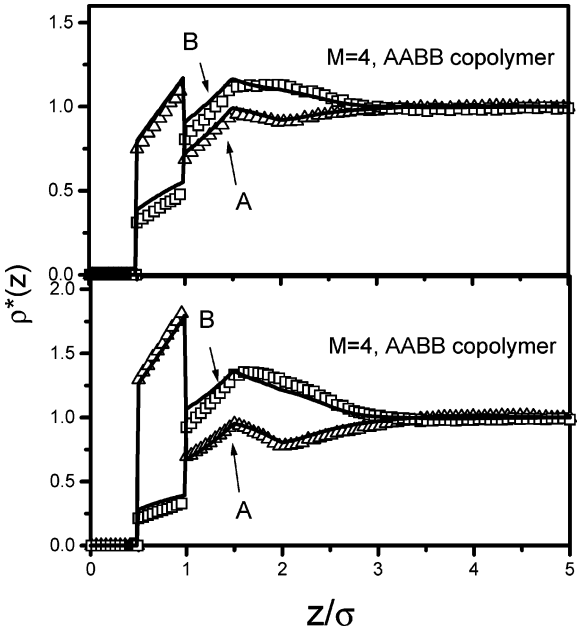

Figure 1. Segmental density profiles of the AABB ($M = 4$) copolymers confined in selective slit pores. The reduced surface energies are (a) $\epsilon^*_{WA} = 0.5$, $\epsilon^*_{WB} = -0.5$; (b) $\epsilon^*_{WA} = 1.0$, $\epsilon^*_{WB} = -1.0$. The packing fraction of copolymers in the pore is $\eta = 0.1$, and the reduced energy parameters are given by $\epsilon^*_{AA} = 1.0$, $\epsilon^*_{AB} = -0.5$, $\epsilon^*_{BB} = 0.5$. The points are from configurational-bias MC simulation, and the lines are from DFT.

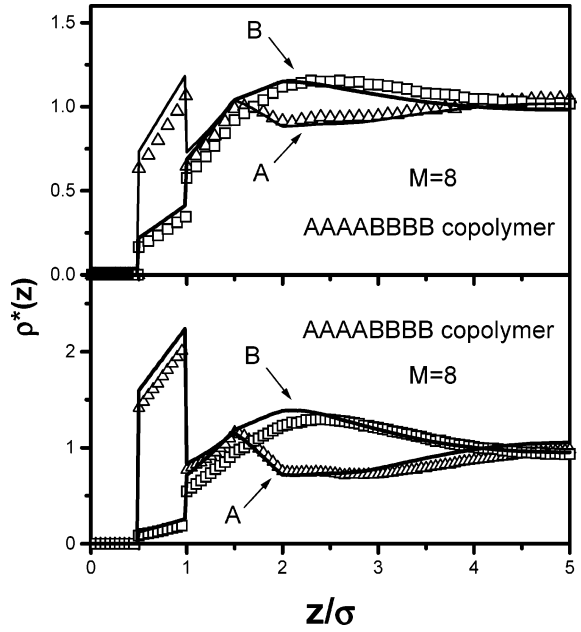

Figure 2. Same as Figure 1 but for the AAAABBBB copolymers.

pore is fixed at $\eta = 0.1$ and the pore width is $H = 10\sigma$. For comparison with simulation data, the corresponding results from DFT are calculated by adjusting the bulk packing fractions such that the predicted average packing factions inside the pore match the conditions of canonical ensemble Monte Carlo simulations.

5.1. AB Diblock Copolymers. We first consider symmetric diblock copolymers represented by "AABB" and "AAAABBBB" confined in slit pores with weakly selective walls, ($\epsilon^*_{WA} = 0.5$, $\epsilon^*_{WB} = -0.5$) and ($\epsilon^*_{WA} = 1.0$, $\epsilon^*_{WB} = -1.0$). Throughout this work, all reduced energy parameters are defined as $\epsilon^* \equiv \beta\epsilon$, and the reduced density is defined as $\rho^*(z) = \rho(z)/\rho_{ave}$, where ρ_{ave} is the average density of segments in the pore. Here a negative energy means repulsion and a positive sign for attractive interactions. The interactions between like segments ("AA" or "BB") are assumed to be energetically favorable ($\epsilon^*_{AA} > 0$ and $\epsilon^*_{BB} > 0$) and that between unlike segments is unfavorable ($\epsilon^*_{AB} = \epsilon^*_{BA} < 0$). We assume further that the attraction between "AA" segments is stronger than that between "BB" segments so that the copolymers may form micelles in the bulk phase.

Figure 1 depicts the segmental density profiles of "AABB" copolymers calculated independently from Monte Carlo simulations and from the DFT. The agreement between DFT and simulation is excellent. As expected, the density profile of "A" segments within the attractive well is always greater than that of "B" segments. Less intuitive though is that the density profiles within the range of surface potential increase with the distance from the surface, and they exhibit a discontinuity at the position where the surface attraction/repulsion terminates. Similar behavior has been reported for monomeric SW fluids near a SW wall.[58,59] For the distributions of "A" and "B" segments beyond the range of the surface potential, the local density of "B" segments is always larger than that of the "A" segments and that difference increases with the surface selective. Both "A" and "B" density profiles present a peak at $z/\sigma = 1.5$, reflecting the packing effect of individual segments. Beyond approximately one layer of molecules (here $z/\sigma = 3.0$), the system becomes essentially homogeneous. Interestingly, the inhomogeneous copolymer layer near the surface correspond to approximately a monolayer of "A" segments followed by fully stretched "B" segments toward the pore center. Nevertheless, the density profiles indicate that there is no sharp separation between "A" and "B" segments.

Figure 2 shows a similar case except that the copolymer has eight segments. A comparison between Figures 1 and 2 indicates that with the same packing fraction and energy parameters the segregation between "A" and "B" segments at the selective surface is magnified as the chain length increases. While the density profiles for the "A" segments show a peak at $z/\sigma = 1.5$ due to the packing effect, the peak for "B" segments occurs at $z/\sigma = 2.0$. In addition, Figure 2 indicates that the range of surface inhomogeneity is slightly less that corresponding to a monolayer of "A" segments plus fully stretched "B" segments. This suggests the coiling of longer chains. Clearly, the results from DFT and MC shown in both Figures 1 and 2 are in quantitative agreement.

5.2. Copolymers with End Site Preferring to the Wall. We now consider the microstructures of copolymers with the end sites preferred to the slit walls. Again, two types of block copolymers, represented by "ABBBBA" and "ABBBBBBA", are examined using both DFT and MC simulations. When the slit pore is weakly selective, i.e., the surface energy is less than one kT for each segment, the density profiles for both A and B segments are similar to those for symmetric diblock copolymers (Figure 3). In comparison with Figures 1 and 2, the only noticeable difference is that the density profile for segment "A" presents only one peak near the surface, and it decays linearly to the bulk value beyond the range of the surface potential. The similarity between the density profiles of the "B" segments in the symmetric and end-active copolymers suggests that

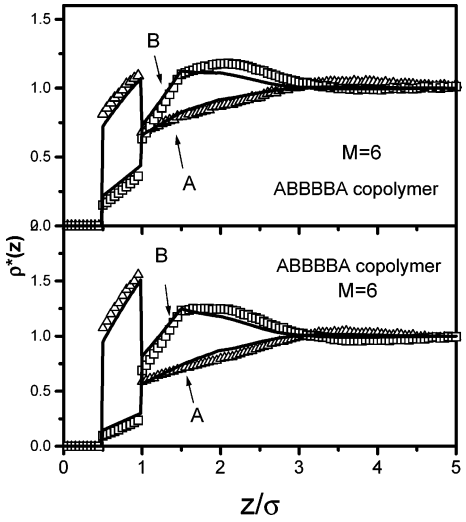

Figure 3. Same as Figure 1 but for the ABBBBA copolymers.

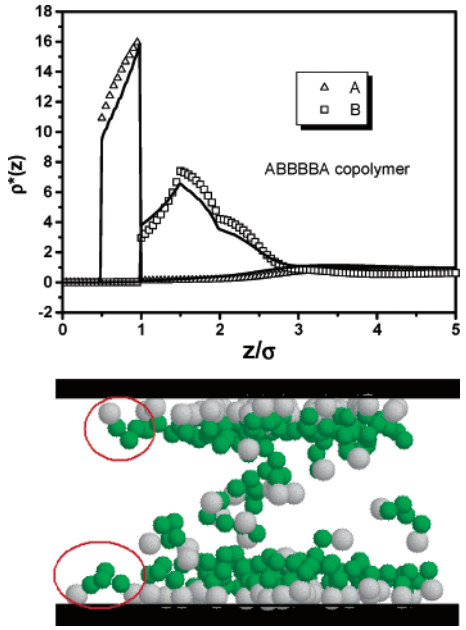

Figure 4. (a) Segmental density profiles and (b) a simulation snapshot of ABBBBA copolymers confined in slit pore with strongly selective walls: $\epsilon^*_{WA} = 5.0$, $\epsilon^*_{WB} = -5.0$

when the surface energy is weak, most copolymers are adsorbed only by one end. However, the situation is different when the surface energy is significantly higher. As shown in Figure 4, when the surface strongly attracts "A" but repels "B" ($\epsilon^*_{WA} = 5.0$, $\epsilon^*_{WB} = -5.0$), the local density of "A" segments within the range of the surface potential is more than 10 times its bulk value. Figure 4b shows a snapshot from Monte Carlo simulation, in which the surface layer is predominately occupied by "A" segments and essentially no "B" segments appear within the range of the surface potential. Because the wall attracts "A" segments but repels the "B" segments, most end-active copolymers form "U"-shape configurations near the surface, which can be clearly observed in Figure 4b. For the guidance of the eye, the circles in the snapshot identify two loop structures.

Figure 5 shows a similar case for end-active copolymers except that the chain length is slightly longer. As expected, an increase of the chain length leads to a broader range of surface inhomogeneity. Similar "U"-shaped configurations appear near the discriminating

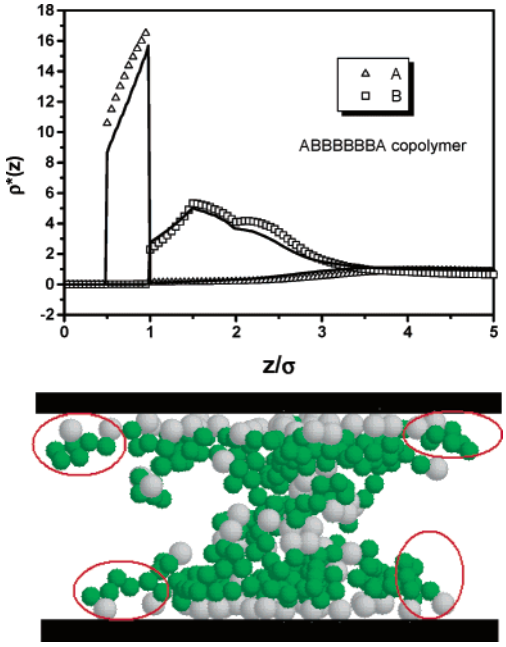

Figure 5. Same as Figure 4 but for ABBBBBBA copolymers.

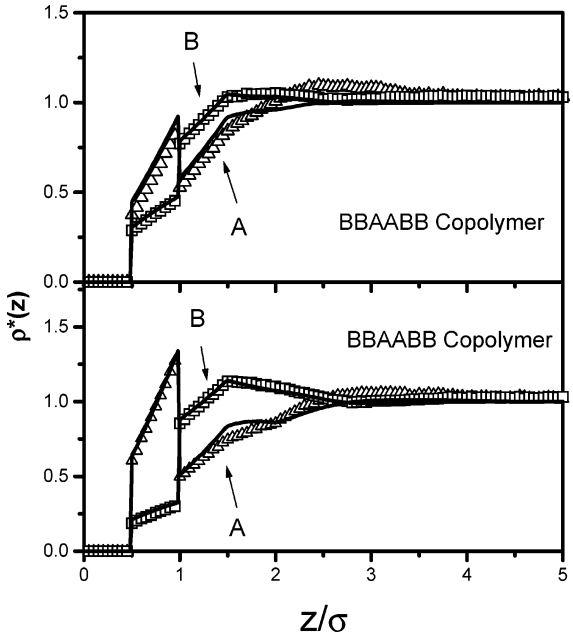

Figure 6. Same as Figure 1 but for the BBAABB copolymers.

surface. Compared with symmetric diblock copolymers, the coiling and folding of chains become more apparent when the chain length increases.

5.3 Triblock Copolymers with Middle Sites Preferred to the Surface. The DFT is easily applicable to copolymer chains of arbitrary structures without significantly increasing the computational complexity. To illustrate, we consider copolymers with the sequences represented by "BBAABB" and "BBBBAABBBB" confined in the slit pores. Figure 6 presents the segmental density profiles of the "BBAABB" copolymers near a weakly selective surface. Because of the entropic restrictions for the middle sites of the polymer chain, the local density of "A" segments within the range of surface potential is much lower than that corresponding to diblock or end-active copolymers at similar conditions. When the surface shows stronger selection between "A" and "B" segments, however, the copolymers form new

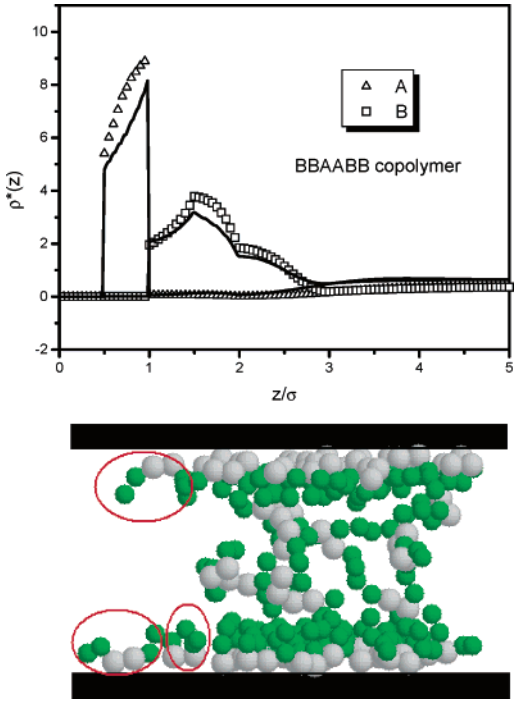

Figure 7. (a) Segmental density profiles and (b) a snapshot of BBAABB triblock copolymers confined in slit pore with strongly selective walls.

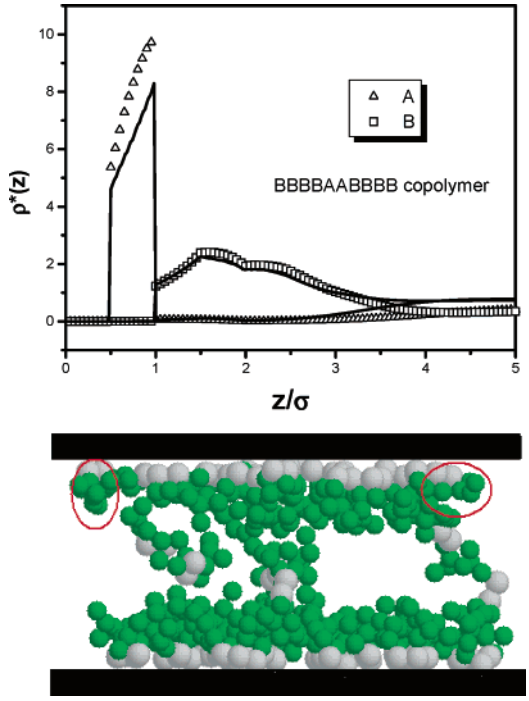

Figure 8. Same as Figure 7 but for BBBBAABBBB copolymers.

"U"-shaped configurations with the open ends pointing toward the pore center. Figure 7 presents the segmental density profiles and a snapshot of the "BBAABB" copolymers. In this case, the surface energy dominates, and most "A" segments adsorb on the surface. The range of inhomogeneity is about 3 times the segment diameter, suggesting that most "B" segments are perpendicular to the surface.

Figure 8 gives the segmental density profiles and a Monte Carlo snapshot of the "BBBBAABBBB" copolymers near a strongly selective surface. Apparently, an

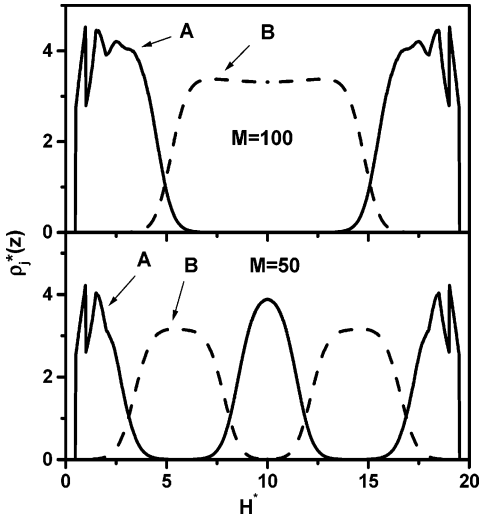

Figure 9. Same as Figure 1 but for the diblock copolymers in slit pore of $H^* = 20$: (a) $M = 100$ (top panel), (b) $M = 50$ (bottom panel).

increase in the chain length expands the range of inhomogeneity near the surface. Furthermore, the coiling and folding of polymer chains become more distinct, which can be clearly observed from the snapshot shown in Figure 8b. For systems with strong surface potential, the DFT slightly underestimates the density profiles of the "A" segments within the range of surface interactions, leading to a small discrepancy in the density far from the surface. This is because the same average segmental density is used in both theory and simulations. It is worth mentioning that when the middle segments are adsorbed onto the wall, the density profiles for the end segments have a shape similar to that for tethered chains.[60]

5.4. Application of the DFT for Longer Chains. For the calibration of the numerical performance of the DFT, we focus only on relatively short chains because it is rather time-consuming to attain reliable molecular simulation data for longer copolymers. However, the application of DFT is definitely not limited to systems containing surfactant-like molecules. Unlike that in simulations, the computational time of DFT for tangent chains increases only linearly with the number of segments. To illustrate, Figure 9 depicts the density profiles of two diblock copolymers of much longer chain length ($M = 50$ and 100) confined in the slit pore of $H^* = 20$. Except the chain length, here all the molecular parameters are the same as those used in Figure 1. Interestingly, we observe lamellar microstructures parallel to the surface for both cases. Intuitively, this can be understood that the copolymers must adjust the chain configurations to fit into the confined spaces when the chain length is greater than the pore width. Therefore, a trilayer ordered film is formed for the diblock copolymer of $M = 100$, and a five-layer lamellar film is formed for the diblock copolymer of $M = 50$. Figure 9 indicates that both the number of layers within the pore and the layer thickness are directly related to the chain length. The formation of lamellar microstructure has been previously reported by both theory[27,49] and experiments.[10]

6. Conclusions

We have presented a new density functional theory (DFT) for block copolymers and demonstrated its nu-

merical performance by extensive comparison with results from configurational-bias Monte Carlo simulations for a variety of tangent square-well chains confined in selective slit pores. The DFT faithfully reproduces the simulation data for the density profiles of individual segments. Even though only a simple coarse-grained model and relatively short copolymer chains are considered in this work, similar procedures should be applicable to more sophisticated models retaining the chemical details. Because of the simplicity and numerical efficiency of the present DFT in comparison with molecular simulations, its applications to more realistic copolymer systems are expectable.

For those systems containing relatively short copolymers (Figures 1−8), we find that the incompatibility parameter χM is in the range of $3 \leq \chi M \leq 5$, less than the critical value of order−disorder transition ($13.5 \leq \chi M \leq 17$),[27] where χ is the Flory−Huggins parameter and M is the total number of segments. As a result, these systems are expected in the disorder state in the bulk phase. However, for systems containing long copolymer chains (Figure 9), the incompatibility parameter is 25 for $M = 50$ and 50 for $M = 100$. For those cases, the systems are likely in the ordered state in the bulk phase. Indeed, as shown in Figure 9, lamellar structures are observed in the slit pores.

Some interesting surface structures are also observed. For example, both simulation and DFT show that the density profiles exhibit a discontinuity at the position when the surface potential terminates. When the block copolymers are adsorbed to a surface by one type of preferential segments, the tangling segments are fully stretched for short chains but coiling and folding for long chains. For the copolymers with the end sites strongly preferred to the surface, we find a special conformation of the "U"-shape with the open ends attached to the surface. However, for copolymers with the middle sites preferred to the wall, the conformation is opposite with the open ends pointing toward the center of the slit pore. We also find that the morphology of copolymer chains is highly sensitive to the chain length. For relatively short chains, a random phase is observed within the channel, but at similar conditions, the copolymers may self-organize into lamellar structures as the chain length increases.

Acknowledgment. The research has been supported by the National Science Foundation (CTS0406100 and CTS0340948).

References and Notes

(1) Binder, K. *Polym. Confined Environ.* **1999**, *138*, 1.
(2) Fasolka, M. J.; Mayes, A. M. *Annu. Rev. Mater. Res.* **2001**, *31*, 323.
(3) Hwang, M. L.; Prud'homme, R. K.; Kohn, J.; Thomas, J. L. *Langmuir* **2001**, *17*, 7713.
(4) Yang, B. S.; Lal, J.; Kohn, J.; Huang, J. S.; Russel, W. B.; Prud'homme, R. K. *Langmuir* **2001**, *17*, 6692.
(5) Hamley, I. W. *Nanotechnology* **2003**, *14*, R39.
(6) Leibler, L. *Macromolecules* **1980**, *13*, 1602.
(7) Helfand, E. *Acc. Chem. Res.* **1975**, *8*, 295.
(8) Bates, F. S.; Fredrickson, G. H. *Annu. Rev. Phys. Chem.* **1990**, *41*, 525.
(9) Fredrickson, G. H. *Macromolecules* **1987**, *20*, 2535.
(10) Anastasiadis, S. H.; Russell, T. P.; Satija, S. K.; Majkrzak, C. F. *Phys. Rev. Lett.* **1989**, *62*, 1852.
(11) Evers, O. A.; Scheutjens, J. M. H. M.; Fleer, G. J. *Macromolecules* **1990**, *23*, 5221.
(12) Evers, O. A.; Scheutjens, J. M. H. M.; Fleer, G. J. *J. Chem. Soc., Faraday Trans.* **1990**, *86*, 1333.
(13) Shull, K. R. *Macromolecules* **1993**, *26*, 2346.
(14) Lyatskaya, Y.; Gersappe, D.; Gross, N. A.; Balazs, A. C. *J. Phys. Chem.* **1996**, *100*, 1449.
(15) Shull, K. R.; Mayes, A. M.; Russell, T. P. *Macromolecules* **1993**, *26*, 3929.
(16) Pickett, G. T.; Balazs, A. C. *Macromolecules* **1997**, *30*, 3097.
(17) Matsen, M. W. *J. Chem. Phys.* **1997**, *106*, 7781.
(18) Suh, K. Y.; Kim, Y. S.; Lee, H. H. *J. Chem. Phys.* **1998**, *108*, 1253.
(19) Petera, D.; Muthukumar, M. *J. Chem. Phys.* **1998**, *109*, 5101.
(20) Huinink, H. P.; Brokken-Zijp, J. C. M.; van Dijk, M. A.; Sevink, G. J. A. *J. Chem. Phys.* **2000**, *112*, 2452.
(21) Huinink, H. P.; van Dijk, M. A.; Brokken-Zijp, J. C. M.; Sevink, G. J. A. *Macromolecules* **2001**, *34*, 5325.
(22) Chen, H. Y.; Fredrickson, G. H. *J. Chem. Phys.* **2002**, *116*, 1137.
(23) Aoyagi, T.; Honda, T.; Doi, M. *J. Chem. Phys.* **2002**, *117*, 8153.
(24) Knoll, A.; Horvat, A.; Lyakhova, K. S.; Krausch, G.; Sevink, G. J. A.; Zvelindovsky, A. V.; Magerle, R. *Phys. Rev. Lett.* **2002**, *89*. 035501.
(25) He, X. H.; Liang, H. J.; Huang, L.; Pan, C. Y. *J. Phys. Chem. B* **2004**, *108*, 1731.
(26) Horvat, A.; Lyakhova, K. S.; Sevink, G. J. A.; Zvelindovsky, A. V.; Magerle, R. *J. Chem. Phys.* **2004**, *120*, 1117.
(27) Geisinger, T.; Muller, M.; Binder, K. *J. Chem. Phys.* **1999**, *111*, 5241.
(28) Chandler, D.; McCoy, J. D.; Singer, S. J. *J. Chem. Phys.* **1986**, *85*, 5971.
(29) Kierlik, E.; Rosinberg, M. L. *J. Chem. Phys.* **1992**, *97*, 9222.
(30) Woodward, C. E. *J. Chem. Phys.* **1991**, *94*, 3183.
(31) Melenkevitz, J.; Muthukumar, M. *Macromolecules* **1991**, *24*, 4199.
(32) McMullen, W. E.; Freed, K. F. *J. Chem. Phys.* **1990**, *93*, 9130.
(33) Frink, L. J. D.; Salinger, A. G.; Sears, M. P.; Weinhold, J. D.; Frischknecht, A. L. *J. Phys.: Condens. Matter* **2002**, *14*, 12167.
(34) Yu, Y. X.; Wu, J. Z. *J. Chem. Phys.* **2002**, *117*, 2368.
(35) Yu, Y. X.; Wu, J. Z. *J. Chem. Phys.* **2003**, *118*, 3835.
(36) Yethiraj, A. *Adv. Chem. Phys.* **2002**, *121*, 89.
(37) McCoy, J. D.; Ye, Y.; Curro, J. G. *J. Chem. Phys.* **2003**, *117*, 2975.
(38) Gotze, I. O.; Harreis, H. M.; Likos, C. N. *J. Chem. Phys.* **2004**, *120*, 7761.
(39) Forsman, J.; Woodward, C. E. *J. Chem. Phys.* **2004**, *120*, 506.
(40) Bryk, P.; Sokolowski, S. *J. Chem. Phys.* **2004**, *120*, 8299.
(41) Bryk, P. *Phys. Rev. E* **2003**, *68*, 062501.
(42) Schweizer, K. S.; Curro, J. G. *Adv. Chem. Phys.* **1997**, *98*, 1.
(43) Cao, D. P.; Wu, J. Z. *J. Chem. Phys.* **2004**, *121*, 4210.
(44) Fredrickson, G. H.; Ganesan, V.; Drolet, F. *Macromolecules* **2002**, *35*, 16.
(45) Fraaije, J. *J. Chem. Phys.* **1993**, *99*, 9202.
(46) Napari, I.; Laaksonen, A.; Strey, R. *J. Chem. Phys.* **2000**, *113*, 4476.
(47) Nath, S. K.; McCoy, J. D.; Curro, J. G.; Saunders, R. S. *J. Chem. Phys.* **1997**, *106*, 1950.
(48) Nath, S. K.; Nealey, P. F.; de Pablo, J. J. *J. Chem. Phys.* **1999**, *110*, 7483.
(49) Frischknecht, A. L.; Curro, J. G.; Frink, L. J. D. *J. Chem. Phys.* **2002**, *117*, 10398.
(50) Napari, I.; Laaksonen, A.; Strey, R. *J. Chem. Phys.* **2000**, *113*, 4480.
(51) Yu, Y. X.; Wu, J. Z. *J. Chem. Phys.* **2003**, *119*, 2288.
(52) Yu, Y. X.; Wu, J. Z. *J. Chem. Phys.* **2002**, *117*, 10156.
(53) Rosenfeld, Y. *J. Phys.: Condens. Matter* **2002**, *14*, 9141.
(54) Chandler, D.; Pratt, L. R. *J. Chem. Phys.* **1976**, *65*, 2925.
(55) Wertheim, M. S. *J. Stat. Phys.* **1984**, *35*, 19.
(56) Frenkel, D.; Smit, B. *Understanding Molecular Simulation;* Academic Press: San Diego, 2002.
(57) Semler, J. J.; Genzer, J. *J. Chem. Phys.* **2003**, *119*, 5274.
(58) Zhou, S. Q. *J. Phys. Chem. B* **2003**, *107*, 3585.
(59) Henderson, J. R.; van Swol, F. *J. Chem. Phys.* **1988**, *89*, 5010.
(60) Ye, Y.; McCoy, J. D.; Curro, J. G. *J. Chem. Phys.* **2003**, *119*, 555.

MA048394S